Hindawi
Geofluids
Volume 2022, Article ID 7150916, 10 pages
https://doi.org/10.1155/2022/7150916

Research Article

Synthetic Method and Oil Displacement Capacity of Nano-MoS_2

Liang Zhang,[1,2] **Fujian Zhou**,[1,2] **Guofa Lei**,[3] **Bingyu Ge**,[4] **Yuan Li**,[1,2] **Guolin Yu**,[1,2] **Longhao Zhao**,[1,2] **Bojun Li**,[1,2] **and Erdong Yao**[1,2]

[1]*Unconventional Natural Gas Institute, China University of Petroleum at Beijing, 102249, China*
[2]*State Key Laboratory of Petroleum Resource and Prospecting, China University of Petroleum at Beijing, 102249, China*
[3]*No. 5 Gas Production Plant of Petrochina Changqing Oilfield Company, 017300, China*
[4]*No. 1 Gas Production Plant, Petrochina Changqing Oilfield Company, 718500, China*

Correspondence should be addressed to Liang Zhang; georabbit1990@163.com

Received 7 April 2022; Revised 24 May 2022; Accepted 30 June 2022; Published 12 July 2022

Academic Editor: Basim Abu-Jdayil

Nanomaterials can be used to emulsify and reduce the fluid viscosity, reduce pore pressure, and increase injection volume. Therefore, nanomaterials have a great potential in the enhanced oil recovery. However, the current research on nanooil flooding materials mostly focuses on the evaluation of the oil-displacing effect, and the lack of research on the size of the oil-displacing materials for tight oil is obvious. In this work, 1T phase molybdenum disulfide nanosheets were prepared by one-step hydrothermal method, which were further modified with CTAB powders to obtain MoS_2-CTAB nanosheet powders. Combined with SEM, TEM, and AFM methods, the nanosheets were optimized based on the appearance and morphology. The stability, wetting reversal, and oil displacement capacity of selected nanosheets were tested. The results show that the best experimental condition to synthesize small-sized molybdenum disulfide is 200°C in the weak acid environment through 12 h. Due to the steric hindrance effect of the CATB molecule, the size and interlayer gap of MoS_2 nanosheets increased slightly after modification. The layer gap reaches to 0.7 nm, and the number of stacked layers is 3~4 layers. Strong Raman bands are observed at 137 cm^{-1}, 291 cm^{-1}, and 391 cm^{-1}, which indicates that the synthesized product is 1T MoS_2. The modified MoS_2 nanosheets in aqueous solution have better dispersion than the unmodified one. After the Zeta test, it was found that the absolute value after modification became lower, indicating that the modification of nano-MoS_2 was effective. Moreover, the MoS_2-CTAB can complete the wetting reversal within 4 h and make the interfacial tension reach 0.89 mN/m at 0.005 wt%, which greatly reduces the capillary pressure. The enhanced oil recovery effect of MoS_2-CTAB nanosheets increased by 85.7% compared with that before modification and 62.5% higher compared with pure surfactant.

1. Introduction

The recoverable resources of unconventional oil and gas in China are 890×10^8-1260×10^8 t oil and gas equivalent, which is about three times of conventional oil and gas, and the reserves are also huge worldwide [1]. However, unconventional reservoirs have poor physical properties, such as low porosity and permeability. These properties could lead to high starting pressure gradient and insufficient formation energy during waterflooding development. Consequently, the oil and gas recovery rates are low. How to improve unconventional oil and gas recovery is the goal of reservoir reformation [2–8]. Nanotechnology, as a new comprehensive science and technology with wide application [9], can solve the engineering problems in the process of unconventional oil and gas reservoir exploitation. For example, tight reservoirs have poor injectability, bad environmental adaptability, apparent reservoir damage, and large dosage [10–12]. Nanomaterials have small size effects, surface effects, wetting properties, and shear thickening properties, as well as unique thermal, mechanical, magnetic, chemical, and other properties. It can be dispersed into nanoscale particles in water medium, hence can easily enter the small pores of unconventional reservoirs and accelerate the oil displacement

efficiency of liquid phase. Therefore, nanomaterials have a broad application prospect in the field of improving oil and gas recovery [13–15].

Most of the nanomaterials currently used in oil and gas development are spherical particles and have extremely low interfacial tension, which can be adsorbed on the rock surface to change the wettability of the rock surface and improve the oil displacement efficiency. However, spherical nanomaterials have a higher adsorption capacity in the reservoir, resulting in high dosage and low economy. Moreover, it is greatly affected by the salinity of the liquid phase [16, 17]. A sheet-like nanomaterial has recently been developed in a nanoresearch industry laboratory. Compared with spherical nanoparticle materials, it has higher interfacial activity and can maintain a certain interfacial tension and has a climbing-film [18] and Marangoni effect [19], which can effectively displace the residual crude oil such as oil film. Sheet-like nanomaterials can spontaneously aggregate on oil-water interface in porous media. It can realize idiopathic oil search and effectively improve the recovery factor of unconventional reservoirs [20]. In 2016, Luo et al. used nanosheets for enhanced oil recovery for the first time, using graphene-modified nanosheets to displace 130 mD artificial sandstone saturated with crude oil under formation water conditions [21]. It was found that even a low concentration of 0.01 wt%, nanosheets could enhance oil recovery by 21.8%. In 2017, modified nanosheets were used again for secondary oil recovery, and it was found that at an ultralow concentration of 0.005 wt%, the recovery rate was increased by 11.1% compared with waterflooding [21]. In 2020, Hou et al. developed a sheet-like 2D smart nano-"black card," which is about 60 nm ∗ 80 nm of single sheet [20]. The microstructure, wettability, interfacial properties, stability, viscosity reduction, and emulsification were studied. The results show that the nano-"black card" can be uniformly dispersed in the water. It can play multiple functions such as wetting reversal, emulsification, reduction of viscosity, interfacial tension, and pressure; ultimately, the crude oil recovery factor increases by 18.1% [18].

At present, the research on nanooil flooding materials is mostly aimed at the evaluation of the oil displacement effect of the material itself. There is a lack of effective discussion and research on the size of oil displacement materials for tight oil. According to the investigation of the controlling factors of the size of sheet-like molybdenum disulfide nanomaterials, we optimally select the small-sized product. Subsequently, the high specific surface area results in decrease in the dosage and cost. Meanwhile, pore throat blockage can be avoided to the greatest extent, so as to achieve high-efficiency oil displacement.

The synthesis of high-purity nanomolybdenum disulfide can often be achieved by template method, chemical vapor deposition (CVD), electrochemical liquid deposition, and hydrothermal synthesis [22–25]. The hydrothermal method can change the reaction factors by altering the liquid temperature, the strength of the reducing agent, the volume of the liquid, etc., thereby affecting the internal reaction system. This method is commonly thought to be simple, high-yield, and controllable. It can be used to synthesize 1T phase MoS_2 nanosheets by one-step [26], which means the products have complete crystal form, uniform particle size distribution, and good dispersion without high temperature treatment. The 1T phase MoS_2 appears an octahedral structure, which is an intermediate form of the 2H phase and is also thermodynamically unstable. Therefore, to efficiently obtain a large amount of 1T phase MoS_2 with high purity, the same octahedral structure molybdenum trioxide is selected as the molybdenum source to directly grow the target product in water [27]. The sulfur source can be selected from thioacetamide and thiourea. While they provide sulfur source, they can be dissolved in water to generate H_2S, which can be used as reducing agent in the process of hydrothermal reaction. In addition, urea was chosen as the reducing agent, and its weak reducibility played an important role in the formation of 1T phase MoS_2 [27]. Through the research on the size factor of molybdenum disulfide, small-sized nanosheets were screened for modification, so as to avoid the blockage of pore throats to the greatest extent and prepare a nanooil flooding system suitable for tight oil reservoirs.

2. Experiments

2.1. Experimental Materials. The materials used to prepare the nanomolybdenum disulfide in laboratory are molybdenum trioxide, thioacetamide, urea, thiourea, cetyltrimethylammonium bromide (CTAB), Sudan Red III (from Aladdin Company, purity 99.0%), aviation kerosene (from Beijing Aviation Kerosene Co., Ltd. Company), potassium chloride (from McLean, 99% purity), and formation water (Xinjiang Mahu block).

2.2. Preparation of Molybdenum Disulfide. 1T phase pure molybdenum disulfide nanosheets were prepared by one-step hydrothermal method. As shown in Figure 1, disperse 0.17 g of molybdenum trioxide, 1.2 g of thioacetamide, 0.3 g of thiourea, and 1 g of urea together in 100 mL of deionized water. It was quickly transferred to a high temperature and pressure reactor. The reaction temperature and time were set. After the reaction, the products were washed for three times using deionized water and ethanol, setting the rotation speed at 4000 rpm and time for 10 min, respectively. In order to avoid the change of the crystal form of MoS_2 due to high temperature, the MoS_2 nanosheet powders were obtained by vacuum drying in a freeze dryer.

2.3. Modification of Molybdenum Disulfide. The obtained MoS_2 nanosheet powder (0.2 g) was ultrasonically dispersed in 100 mL of deionized water for 10 min, and CTAB powders (1 g) were added to dissolve in the uniform dispersion of nanosheets and stirred at room temperature (25°C) for 24 h. The washing steps in the preparation process were repeated, and the MoS_2-CTAB nanosheet powders were obtained by vacuum drying in a freeze dryer.

2.4. Morphology and Characterization of Molybdenum Disulfide. The morphology of molybdenum disulfide nanosheets was measured and observed by scanning electron microscope (SEM), transmission electron microscope (TEM), and atomic force microscope (AFM). Nanosheets with clear boundaries and small lateral dimensions are

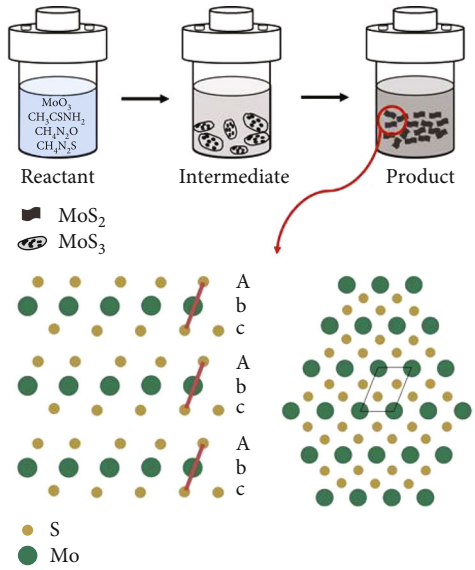

Figure 1: MoS_2 synthetic reaction flow chart.

preferred. The chemical composition and structure of MoS_2 and MoS_2-CTAB nanosheets were analyzed using FTIR and Raman spectroscopy. The wavelength of the excitation light source for Raman spectroscopy is 532 nm, and the spot size is about 1 micron.

2.5. Stability Study of Molybdenum Disulfide. Nanoparticles tend to interconnect after synthesis, which result in forming large particle agglomerates that contain multiple particles. Because of the agglomeration, the dispersion is thermodynamically unstable, which greatly affects the dispersion effect [28]. MoS_2 and MoS_2-CTAB were, respectively, dispersed by ultrasonic wave and dissolved in deionized water. The concentration of the dispersion liquid was 0.005 wt%, and it was placed at room temperature for 3 days, and the sedimentation of the nanomaterials was continuously observed.

2.6. Zeta Potential Analysis. The Zeta potential of two kinds of nanofluids before and after modification was tested by Zetasizer Nano ZS after fully ultrasonically dispersion at a temperature of 20°C.

2.7. Contact Angle and Interface Properties. Changes in the wettability of the core surface by nanomaterial dispersions were tested using oil-wet cores. The artificial dry cores were first pretreated, and the cores were aged in simulated oil for one week, and then, the original contact angles were measured. Then, cores were immersed in nanofluid (0.005 wt%), and the wettability characteristics were observed at 4 h, 8 h, and 12 h, respectively. The oil-water interfacial tension of nanofluids was detected by interfacial tensiometer, and the distribution of nanomaterials at the oil-water interface was observed.

2.8. Core Flooding. To simulate the underground dynamic oil displacement process and study the enhanced oil recovery capability of the nanodisplacement system, the specific experimental steps are as follows.

Table 1: Morphology and size of products at different synthesis temperatures.

Groups	Reaction temperature (°C)	Response time (h)	Shape and size
1	180	12	Indeterminate form
2	200	12	Flake, 22~40 nm
3	220	12	Flake, 60~80 nm
4	240	12	Petal-like, about 200 nm

(1) Configure 2% KCl aqueous solution

(2) At room temperature, add modified MoS_2 nanosheets into KCl aqueous solution to configure 0.005 wt% nanoflooding fluid

(3) Put the dry core in the airtight container for vacuuming, and then inject the simulated formation water to continuous saturation at 20Mpa for one day

(4) Load the core into the core holder. The experimental temperature is 70°C, and the confining pressure of the core is 15 MPa. The simulated oil was injected into the core at a rate of 0.2 mL/min until there was no residual brine. The total volume of drained water is recorded, which is the saturated oil volume

(5) After getting oil-saturated cores, inject 2 wt% KCl (1-3PV) at a rate of 0.2 mL/min until no oil is discharged. In this process, the volume of the discharged oil at the outlet was measured by a measuring cylinder, and divide the volume of the discharged oil by the volume of saturated oil to obtain the recovery rate of KCL

(6) After step (5), inject 1-3PV of nanofluid into the core at a rate of 0.2 mL/min until no oil is discharged. Measure the volume of the discharged oil with a measuring cylinder at the outlet, and divide the volume of the discharged oil by the volume of saturation oil to obtain the recovery factor of nanofluid

3. Results and Discussion

3.1. Preparation and Size Control of Molybdenum Disulfide. In order to study the reaction factors affecting the size of nano-MoS_2 during hydrothermal synthesis, synthesis time, temperature, and pH were selected as single-factor variables. The size distribution was observed by SEM. In this reaction, the crystallization temperature provides the energy for the whole reaction, directly determines the direction of the reaction, and plays an important role in the morphology of the product. Therefore, the effect of synthesis reaction temperature on the material size was first investigated. In previous studies, the temperature of the hydrothermal method is generally 160-300°C, and different temperatures will change the morphology and size of nano-MoS_2 [29]. For the synthesis of flaky nano-MoS_2 materials, the temperature is usually

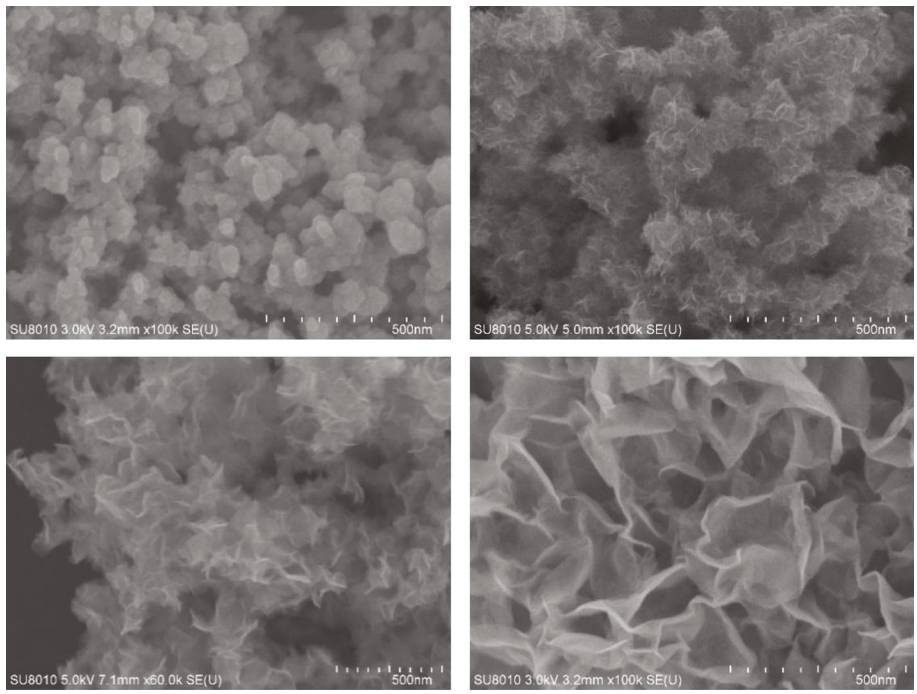

Figure 2: Micrograph of scanning electron microscope showing the morphology of MoS_2 (No. 1, No. 2, No. 3, and No. 4 in turn).

180~240°C, so four temperature gradients of 180°C, 200°C, 220°C, and 240°C were selected for the comparison. The results are shown in the Table 1.

It can be seen from Table 1 and Figure 2 that due to the low temperature and insufficient reducibility, No. 1 products finally showed an indeterminate shape without obvious morphology boundaries (nonlamellar structure). In No. 2, 3, and 4 groups, as the reaction temperature increases, the nano-MoS_2 exhibits lamellar structures, and its size gradually increases. The agglomeration phenomenon, meanwhile, is also more serious. The size of No. 2 group is between 22 and 40 nm, and the morphology is relatively uniform. Therefore, 200°C is the optimum temperature for the formation of small-sized molybdenum disulfide. Studies have shown that the existence of van der Waals forces will attract the aggregation between nanosheets, and the distance between sheets determines the number and stacking of nanosheets [30]. In addition, the growth of crystals in the hydrothermal method is generally divided into two processes of formation and growth of crystal nucleus. Relatively low temperature is conducive to the formation of crystal nucleus. However, high temperature will affect the growth direction of nucleus [31]. Accordingly, as the temperature increases, the overall pressure inside the reaction system increases, the nucleus continues to collide, and the distance between the nanosheets tends to increase gradually. At the same time, the number of folds and bends in a single sheet increases, and the specific surface area increases relatively.

The reaction time also has an important influence on the growth of nanocrystals. It is generally believed that with the increase of the reaction time, the morphology of the nanoproducts will be more complete, the boundary will be clearer, and the crystallinity will increase. Inheriting the chemical ratio and reaction temperature of No. 2, the reaction time was changed to 10 h, 14 h, and 16 h, respectively, and the morphology and size of the product were compared.

Table 2: Morphology and size of products under different reaction time.

Groups	Reaction temperature (°C)	Response time (h)	Shape and size
5	200	10	Indeterminate form
6	200	14	Flake, 90-100 nm
7	200	16	Petal-shaped, about 400 nm

As can be seen from Table 2 and Figure 3, No. 5 is not a sheet-like material, because the reaction time was not long enough; it also appeared indeterminate form. Compared with No. 1, its maturity is low, and it shows a mushy form. When the reaction time reaches 14 h and 16 h, the boundary structure of the nanosheets is gradually clear, and the average size also increases gradually. The largest product is No. 7 with an approximate size of about 400 nm, and the size of a single chip has also increased. Consistent with the general perception, as the reaction time increases, the crystal morphology becomes more regular, the grain accumulation becomes more serious, and the size increases. But at the same time, in the absence of sufficient reaction time, unshaped MoS_2 will be obtained. Therefore, the reaction time of 12 h is the optimal time for the formation of small-sized MoS_2 nanosheets.

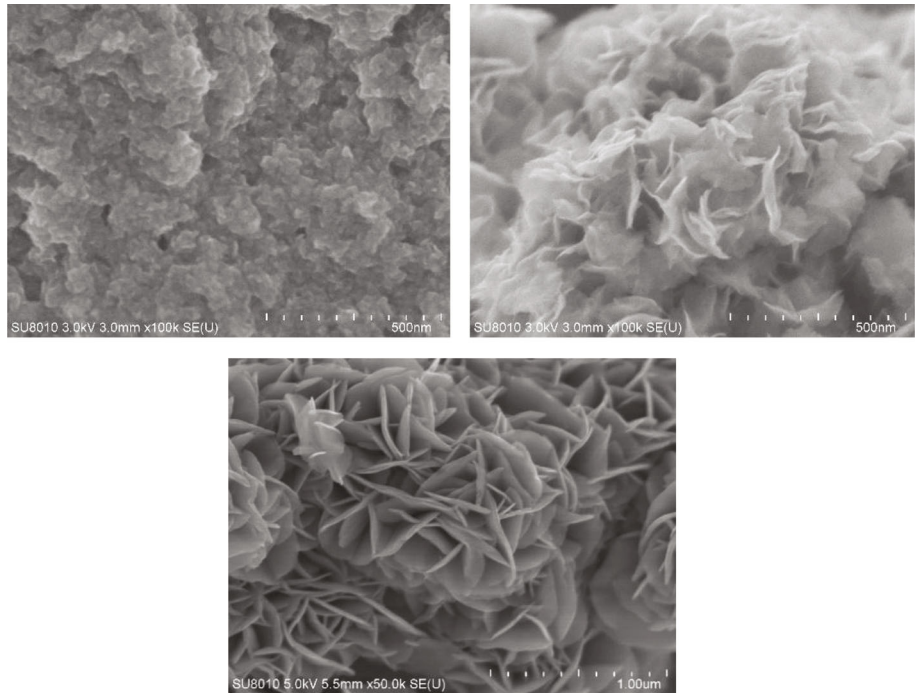

Figure 3: Micrograph of scanning electron microscope showing the morphology of MoS_2 (No. 5, No. 6, and No. 7 in turn).

Table 3: Morphology and size of products under different pH solutions.

Groups	Reaction temperature (°C)	Response time (h)	pH	Shape and size
8	200	12	1	Flake, 30~50 nm
9	200	12	3	Flake, 30~40 nm
10	200	12	6	Flake, 20~35 nm

During the reaction, the pH value of the mixed solution affects the reaction rate by changing the solubility and saturation of the reactants, thereby affecting the formation of crystal nuclei. Since thiourea has reducibility in acidic solution and is unstable in alkaline solution, it is decomposed into S^{2-} and $SC(NH_2)^{2+}$. Similarly, thioacetamide is hydrolyzed in alkaline solution to generate S^{2-} and NH_3, Therefore, the range of pH is set between 1 and 6, and the concentrated hydrochloric acid is used to adjust the pH, as shown in Table 3.

It can be seen from Figure 4 that with the gradual increase of pH, the boundary of the lamellar product becomes clear. At the same time, the size is more uniform. In sample No. 8, a part of the indeterminate form appeared, and the surface was smooth. It shows that the growth direction of the crystal nucleus is affected in a strong acidic environment. Sample No. 9 is more tightly stacked and more complete in morphology, but slightly larger than sample No. 10. Sample No. 10 has a sharp outline, and the lamellar structure is thinner, and its size distribution ranges between 20 nm and 35 nm. Therefore, it is easier to obtain uniform and small-sized MoS_2 nanosheets under weakly acidic conditions.

3.2. Modification and Characteristics. According to the previous study on the influence of synthesis factors on the size of molybdenum disulfide, the No. 10 sample was selected for the modification work and other testing works. The modified No. 10 samples were observed by SEM, TEM, and AFM to further study of its morphological characteristics (Figure 5). SEM and TEM results show that the size and interlayer gap of the modified molybdenum disulfide nanosheets increase slightly, the interlayer gap reaches 0.7 nm, and the number of stacked layers is 3-4 layers. The main reason is that the presence of CATB molecules produces a steric hindrance effect, which hinders the stacking of nanosheets. AFM results show that the height of the stack is 13 nm at the highest point, and its monolayer height is about 3.25 nm, which is also slightly higher than that of pure MoS_2 in the literature (2.88 nm) [32].

Zeta potential can be used to test whether the modification is successful or not. The potential of pure MoS_2 nanosheets presents a high negative value (absolute value greater than 20). As can be seen from Figure 6, the Zeta potential of CTAB-MoS_2 is -3, indicating that the structure of MoS_2 nanosheets modified by CTAB has changed; the amine group of CTAB reacted with the hole or suspension bond of molybdenum disulfide, indicating that the modification was successful.

3.3. Raman Spectroscopy Results. Raman spectroscopy was performed on sample No. 10 and selected for analysis in the range of 100 to 550 cm^{-1}. The biggest difference in structure between 1T and 2H crystals is the symmetry of S atom in unit, which is reflected in the significant difference in

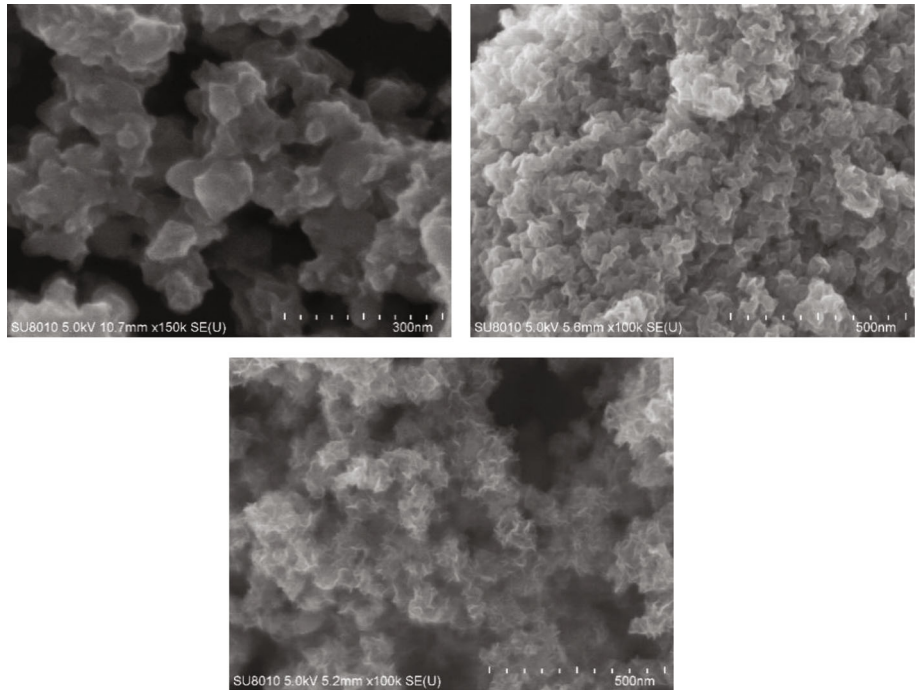

Figure 4: Micrograph of scanning electron microscope showing the morphology of MoS_2 (No. 8, No. 9, and No. 10 in turn).

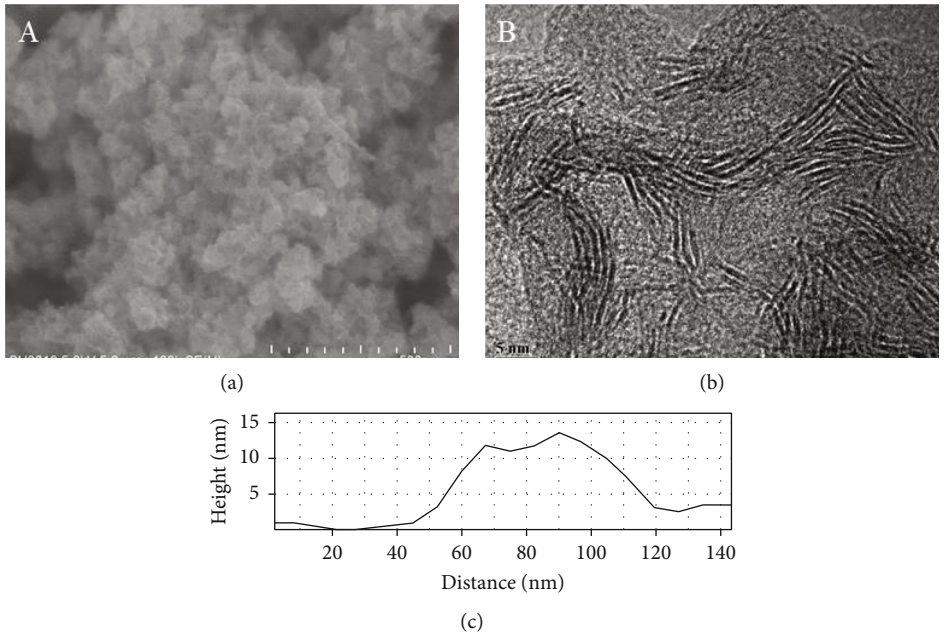

Figure 5: Micrograph of scanning electron microscope (a), transmission electron microscope (b), and result of atomic force microscope (c) of modified sample No. 10.

Raman characteristic peaks [33]. As shown in Figure 7, the results show that strong Raman bands are observed at 137 cm^{-1}, 291 cm^{-1}, and 391 cm^{-1}. Among them, the peaks of 291 cm^{-1} and 391 cm^{-1} correspond to the Mo-S bond which are, respectively, parallel to the layer direction and perpendicular to layer direction. The peak of 137 cm^{-1} is a unique vibration structure of 1T phase, which is mainly attributed to the tensile vibration between Mo-Mo bond, which proves that the synthesized product is 1T type MoS_2 [33, 34].

3.4. Stability Study. The modified MoS_2 nanosheets in aqueous solution have better dispersion stability than that before modification. According to the results shown in Figure 8, the color of the nanodispersion before modification after 3days becomes lighter as light gray-black. Some dark black solid

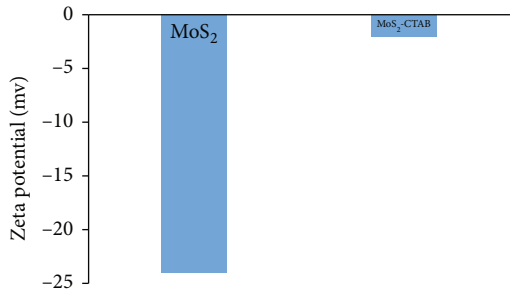

Figure 6: Zeta potential of molybdenum disulfide before and after modification.

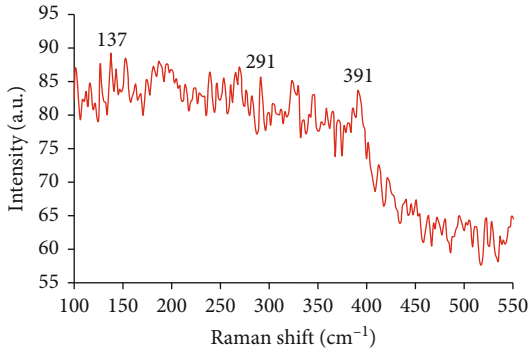

Figure 7: Raman spectroscopy test of MoS_2 nanosheets.

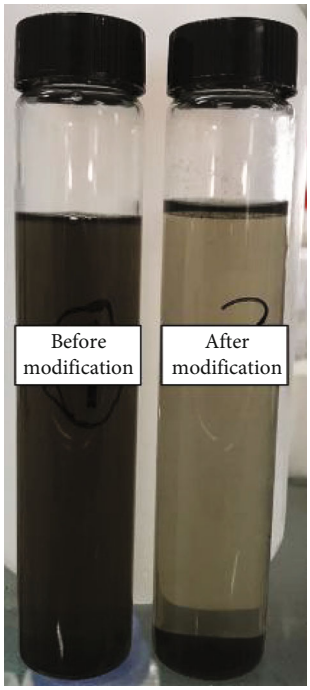

Figure 8: Stability evaluation of modified molybdenum disulfide.

powder appears at the bottom of the bottle. The color of the modified nanodispersion basically remains black, which indicates that it is stable dispersion within 3 days. It is generally believed that the main driving forces for the agglomeration and sedimentation of nanodispersions are the van der Waals force and the electrostatic charge Coulomb force. Especially when the van der Waals force is much greater than the particle's own gravity, the nanoparticles will agglomerate and settle. According to the TEM results, after CTAB modification, the wettability of the particle surface is improved, the attraction energy between particles is reduced, and the repulsion energy between particles is increased, which can effectively form a steric hindrance effect, thereby significantly improving the dispersion performance [35].

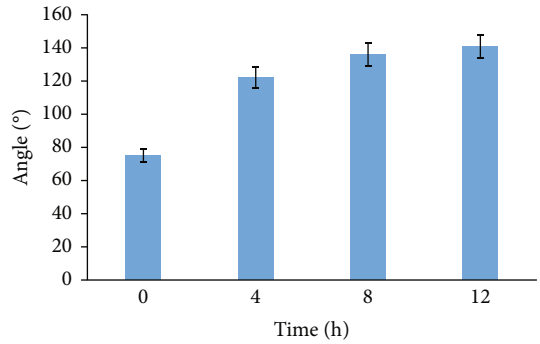

Figure 9: Variation of core contact angle at different times.

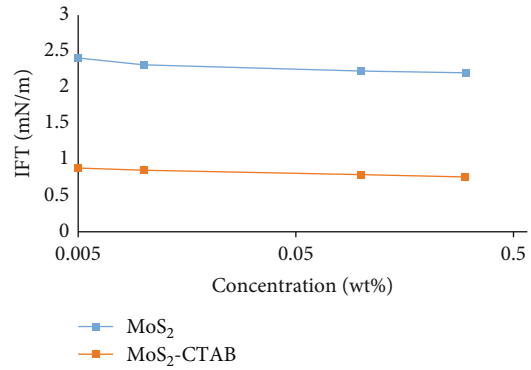

Figure 10: IFT value of nanodispersions with different concentrations.

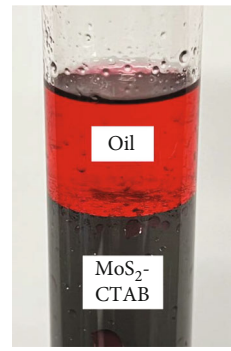

Figure 11: MoS_2-CTAB oil-water interface distribution.

3.5. Wettability Study. Wettability evaluation plays an indispensable role in material flooding research. Stripping the remaining oil by wetting reversal is one of the effective oil

Table 4: Dynamic oil displacement core parameters.

Simple name	Lithology	Length (cm)	Dia (cm)	Permeability (mD)	Porosity (%)	Injecting fluid
JX1	Sandstone	5.01	2.51	7.323	14.72	CTAB
JX2	Sandstone	4.98	2.51	7.641	14.89	MoS_2
JX3	Sandstone	5.13	2.51	7.571	14.77	MoS_2-CTAB

displacement mechanisms of oil displacement materials. Oil droplets are slowly injected at the bottom of the aged core by placing it in water. The change of soaking time on the wettability of the core was studied. The results (Figure 9) show that before soaking in the nanodispersion, the contact angle of the oil droplet at the three-phase boundary interface is 75°, which indicates that the core after aging is pure oil wet. With soaking in the dispersion liquid, the contact angle increases with time from 122°, then 136°, to 141° at 4 h, 8 h, and 12 h, respectively. Meanwhile, we define the soaking time as 4 h for the wettability change, as the improvement is weak with soaking time over 4 h. It shows that MoS_2-CTAB can completely change the wettability in a short time.

3.6. Research on Interface Properties. The oil-water interfacial tension (IFT) of nano-MoS_2 before and after modification at different concentrations was measured to determine the optimum concentration of the dispersion liquid for oil displacement. The results (Figure 10) show that the interfacial tension of MoS_2-CTAB dispersion is significantly lower than that of pure MoS_2. At 0.005 wt%, it can reach 0.89 mN/m, which can greatly reduce the oil-water interface gradient, which is beneficial to improve oil recovery. With the increase of nanomaterial concentration, the IFT of both before- and after-modification dispersion is decreased, but the decrease is not obvious. Therefore, further increasing the concentration of nanomaterials has little effect on the reduction of IFT, and the lowest concentration of 0.005 wt% can be selected for the next indoor dynamic oil displacement experiments.

The kerosene was added into the 0.005 wt% modified dispersion. For the convenience of observation, the kerosene was dyed with red color. As shown in Figure 11, some nanoparticles are stably concentrated in the oil-water interface. It shows that MoS_2-CTAB has the effect of neutral wetting and can realize the wetting reversal, which is consistent with the experimental results of the contact angle.

3.7. Core Flooding Results. The core flooding experiments were performed using different fluids to study the enhanced oil recovery of nanosheets before and after modification. The CTAB was added as a control group to analyze the enhanced oil recovery effect of pure surfactant flooding. The core data of injected nanofluid are shown in Table 4, all of which are artificial tight sandstone. Through laboratory optimization, the cores with a permeability of 5 mD match aperture best. In addition, the injected CTAB solution has the same concentration with the nanofluid which is 0.005 wt%. The waterflooding recovery factors of the three rock samples remained basically unchanged during the first 4 PV injections. Therefore, flooding fluid is injected at the 5 PV, and

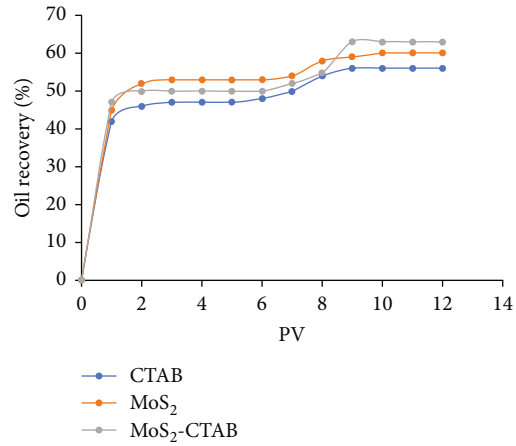

Figure 12: Indoor dynamic oil displacement results.

the final recovery factor is shown in Figure 12. The results show that after waterflooding and injecting the corresponding flooding fluids in JX1 and JX2, the recovery factor increases to approximately 8% and 7%, respectively. In contrast, the recovery factor growth rate of JX3 is about 13%. Before modification, it increases by 85.7%, which was 62.5% higher than that of pure surfactant. Therefore, the oil displacement performance after modification was significantly improved.

The oil displacement mechanism of surfactants is commonly thought as the reduction of the oil-water interfacial tension and the surface free energy of rock formations. It ensures high oil washing efficiency and low degree of emulsification, so as to achieve the purpose of enhanced oil recovery [36]. Using single surfactant flooding is usually inefficient. To obtain a batter performance, the usage of the surfactant flooding is commonly mixed with polymers, alkalis, etc. Therefore, the oil displacement effect on JX1 is relatively bad. Nanoparticles can usually achieve wetting reversal and reduce interfacial tension reduction and wedge flooding, which has been demonstrated in the previous experiments. The modified nanodispersion can further stabilize the nanoparticles and is endowed with both the properties of surfactants and nanoparticles. Therefore, the oil displacement performance is more obvious, and the better dispersion stability can also avoid the premature deposition of nanoparticles, which results in the block of the pore throat. In addition, sheet-like nanomaterials have more unique advantages in the oil displacement. Due to the difference in the hydrophilicity of its bottom and edges, it spontaneously gathers between the interfaces of oil and water in aqueous solutions, similar to surfactants. After modification, the properties of surfactants and nanoparticles promote the

density and activity of the surfactant, thereby greatly improving the oil displacement efficiency.

4. Conclusions

In this work, 1T phase molybdenum disulfide nanosheets were prepared by one-step hydrothermal method, which were further modified using CTAB powders to obtain MoS_2-CTAB nanosheet powders. Combined with SEM, TEM, and AFM methods, the nanosheets were optimized based on the appearance and morphology. The stability, wetting reversal, and oil displacement capacity of selected nanosheets were tested. The conclusions are as follows:

In order to synthesize smaller-sized MoS_2 nanosheets by hydrothermal method, the reaction should be in a weakly acidic environment and taken place at 200°C for 12 hours. The best products can be stabilized at $28\,nm * 50\,nm$. Through Raman spectrum analysis, the synthesized product is proved to be 1T type MoS_2.

CTAB was optimized to modify the product. The existence of CATB molecules produces a steric hindrance effect, which hinders the stacking of nanosheets. In terms of oil displacement capacity, it shows that MoS_2-CTAB can change the wettability completely in a short time and that the interfacial tension of MoS_2-CTAB dispersion is much lower than that of pure MoS_2, and it can reach to 0.89 mN/m at 0.005 wt%, which can greatly reduce the oil-water interface gradient. The enhanced oil recovery rate increased by 85.7% compared with the unmodified products and by 62.5% compared with the pure surfactant. Consequently, the oil displacement effect after modification was significantly improved.

Data Availability

The data that support the findings of this study are available from the corresponding author upon reasonable request.

Conflicts of Interest

The authors declare that they have no conflicts of interest.

Acknowledgments

This research was financially supported by the National Natural Science Foundation of China (Grant Nos. 52004306 and 52174045).

References

[1] Z. Caineng, Y. Zhi, Z. Rukai et al., "Progress in China's unconventional oil & gas exploration and development and theoretical technologies," *Acta Geologica Sinica-English Edition*, vol. 89, no. 3, pp. 938–971, 2015.

[2] L. W. Y. G. Z. Fengde and H. Z. L. Jiefen, "Water displacing oil efficiency with cores grouped in parallel of different flow units in low-permeability reservoirs," *Acta Petrolei Sinica*, vol. 32, no. 4, pp. 658–663, 2011.

[3] H. E. Dou, S. Y. Ma, C. Y. Zou, and S. L. Yao, "Threshold pressure gradient of fluid flow through multi-porous media in low and extra-low permeability reservoirs," *Science China Earth Sciences*, vol. 57, no. 11, pp. 2808–2818, 2014.

[4] Z. Rukai, W. Songtao, S. Ling, C. Jingwei, M. Zhiguo, and Z. Xiangxiang, "Problem sand future works of porous texture characterization of tight reservoirs in China," *Acta Petrolei Sinica*, vol. 37, no. 11, pp. 1323–1336, 2016.

[5] H. Wenrui, W. Yi, and B. Jingwei, "Development of the theory and technology for low permeability reservoirs in China," *Petroleum Exploration and Development*, vol. 45, no. 4, pp. 125–137, 2018.

[6] L. Huan, W. Qingbin, G. L. Du Xiaofeng, Y. Ge, W. Xiabin, and L. Junzhao, "Low-permeability reservoir types classification and reservoir sensitivity controlling factors: a case study of Paleogene in Bohai Sea," *Acta Petrolei Sinica*, vol. 40, no. 11, pp. 1331–1345, 2019.

[7] L. Xiangfang, F. Dong, Z. Tao et al., "The role and its application of capillary force in the development of unconventional oil and gas reservoirs and its application," *Acta Petrolei Sinica*, vol. 41, no. 12, pp. 1719–1733, 2020.

[8] F. Y. Wang, F. C. Zeng, and J. Y. Zhao, "A mathematical model of displacement and imbibition of low- permeability/tight reservoirs and its application," *Acta Petrolei Sinica*, vol. 41, no. 11, pp. 1396–1405, 2020.

[9] S. Shuang, X. Yang, and Y. Zhou, "New research progress on preparation and application of Janus particles," *Journal of Shanxi University*, vol. 40, no. 3, pp. 577–589, 2017.

[10] Z. Wenzhong, H. Yufeng, W. Bin, X. Yubing, S. Pengfei, and W. Rongmin, "Fabrication and applications of polymeric Janus particles," *Progress in Chemistry*, vol. 29, no. 1, pp. 127–136, 2017.

[11] L. Jianhui, Y. Jie, L. Yuanyang, H. Lipeng, and J. Bo, "Synthesis of amphiphilic silica nanoparticles with double-sphere morphology," *Chemical Journal of Chinese Universities*, vol. 39, no. 10, pp. 2170–2177, 2018.

[12] L. E. I. Qun, L. U. O. Jianhui, P. E. N. G. Baoliang et al., "Mechanism of expanding swept volume by nano-sized oil-displacement agent," *Petroleum Exploration and Development*, vol. 46, no. 5, pp. 991–997, 2019.

[13] J. H. Luo, Y. L. Zhang, B. W. Yang, Y. E. Long-Qiang, B. Ding, and B. Jiang, "Preparation of hydrophobic silica nanoparticles with different size by sol-gel technology," *Chemical Research Application*, vol. 25, no. 8, pp. 1136–1139, 2013.

[14] L. U. O. Jianhui, D. I. N. G. Bin, Y. A. N. Youguo et al.Molecular dynamics simulation of adsorption behavior of alkyl-modified SiO_2 nanoparticles at oil/water interface," *Journal of China University of Petroleum*, vol. 39, no. 2, pp. 130–136, 2015.

[15] L. He, J. Luo, B. Ding, P. Wang, and Y. Li, "Preparation and properties of nano oil displacement agent for low/ultra-low permeability reservoir," *Oilfield Chemistry*, vol. 35, no. 1, pp. 81–84, 2018.

[16] N. A. Ogolo, O. A. Olafuyi, and M. O. Onyekonwu, *Enhanced Oil Recovery Using Nanoparticles, in SPE Saudi Arabia Section Technical Symposium and Exhibition*, Enhanced Oil Recovery Using Nanoparticles, Saudi Arabia, 2012.

[17] I. Raj, M. Qu, L. Xiao et al., "Ultralow concentration of molybdenum disulfide nanosheets for enhanced oil recovery," *Fuel*, vol. 251, pp. 514–522, 2019.

[18] J. B. Yang, J. R. Hou, M. Qu et al., "Evaluation of oil displacement performance of two-dimensional smart black nano-card in low permeability reservoir," *Oilfield Chemistry*, vol. 37, no. 2, pp. 305–310, 2020.

[19] C. Bin, L. Weidong, and S. Linghui, "Study of Marangoni convection experiment between crude oil and chemical flooding systems," *China Surfactant Detergent & Cosmetics*, vol. 41, no. 5, pp. 318–321, 2011.

[20] H. O. U. Jirui, W. E. N. Yuchen, and Q. U. Ming, "Research and application of nano-materials to enhance oil and gas recovery technology," *Special Oil and Gas Reservoirs*, vol. 27, no. 6, pp. 47–53, 2020.

[21] D. Luo, F. Wang, J. Zhu et al., "Nanofluid of graphene-based amphiphilic Janus nanosheets for tertiary or enhanced oil recovery: high performance at low concentration," *Proceedings of the National Academy of Sciences of the United States of America*, vol. 113, no. 28, pp. 7711–7716, 2016.

[22] Y. Ni, M. Xiang, and J. Hong, "Microwave-assisted template synthesis of an array of CdS nanotubes," *Materials Letters*, vol. 58, pp. 2754–2756, 2004.

[23] M. A. Lukowski, A. S. Daniel, F. Meng, A. Forticaux, L. Li, and S. Jin, "Enhanced hydrogen evolution catalysis from chemically exfoliated metallic MoS_2 nanosheets," *Journal of the American Chemical Society*, vol. 135, no. 28, pp. 10274–10277, 2013.

[24] Y. Yu, C. Li, Y. Liu, L. Su, Y. Zhang, and L. Cao, "Controlled scalable synthesis of uniform, high-quality monolayer and few-layer MoS2 films," *Scientific Reports*, vol. 3, no. 1, pp. 1866–1872, 2013.

[25] B. Chen, Q. Yu, Q. Yang et al., "Large-area high quality MoS2 monolayers grown by sulfur vapor counter flow diffusion," *RSC Advances*, vol. 6, no. 55, pp. 50306–50314, 2016.

[26] C. Cai, F. Wu, and Y. Fang, "Hydrothermal synthesis of flower-like MoS2 nanoparticle," *Hans Journal of Nanotechnology*, vol. 3, no. 2, pp. 19–23, 2013.

[27] X. Geng, W. Sun, W. Wu et al., "Pure and stable metallic phase molybdenum disulfide nanosheets for hydrogen evolution reaction," *Nature Communications*, vol. 7, no. 1, article 10672, 2016.

[28] H. B. Liu, *The Research on Modification on Oxides Nano-Particles and Its Applications*, Hunan University, China, 2012.

[29] Y. Tian, Y. He, and Y. Zhu, "Low temperature synthesis and characterization of molybdenum disulfide nanotubes and nanorods," *Materials Chemistry Physics*, vol. 87, no. 1, pp. 87–90, 2004.

[30] G. T. Zhou, *Fabrication of MoS2 Thin Film and Research on the Application of Solar Cells*, Huazhong University of Science & Technology, China, 2019.

[31] T. L. Ming, *Nano molybdenum disulfide materials synthesized by hydrothermal method*, Northwest University, Washington, 2014.

[32] M. Qu, J. Hou, T. Liang et al., "Preparation and interfacial properties of ultralow concentrations of amphiphilic molybdenum disulfide nanosheets," *Industrial & Engineering Chemistry Research*, vol. 59, no. 19, pp. 9066–9075, 2020.

[33] S. J. Sandoval, D. Yang, R. F. Frindt, and J. C. Irwin, "Raman study and lattice dynamics of single molecular layers of MoS2," *Physical Review B*, vol. 44, no. 8, pp. 3955–3962, 1991.

[34] T. J. Wieting and J. L. Verble, "Infrared and Raman studies of long-wavelength optical phonons in hexagonal MoS2," *Physical Review B*, vol. 3, no. 12, pp. 4286–4292, 1971.

[35] B. X. TIan, *Application of nanofluid in EOR and its mechanism*, China University of Petroleum, East, China, 2017.

[36] F. Gao and Z. Z. Song, "Mechanism of surfactant flooding in low-permeability oilfields," *Journal of China University of Petroleum*, vol. 36, no. 4, pp. 160–165, 2012.